# Atlantic Warm Pool Acting as a Link between Atlantic Multidecadal Oscillation and Atlantic Tropical Cyclone Activity

Chunzai Wang[1]
Sang-Ki Lee[1, 2]
David B. Enfield[1]

[1] NOAA Atlantic Oceanographic and Meteorological Laboratory
Miami, Florida

[2] Cooperative Institute for Marine and Atmospheric Studies
University of Miami
Miami, Florida

Special Issue of $G^3$ Focusing on
"Interactions Between Climate and Tropical Cyclones on All Time Scales"

March 2008

Corresponding author address: Dr. Chunzai Wang, NOAA/AOML, 4301 Rickenbacker Causeway, Miami, FL 33149. E-mail: Chunzai.Wang@noaa.gov.

## Abstract

Multidecadal variability of Atlantic tropical cyclone activity is observed to relate to the Atlantic Multidecadal Oscillation (AMO) – a mode manifesting primarily in sea surface temperature (SST) in the high latitudes of the North Atlantic. In the low latitudes of the North Atlantic, a large body of warm water called the Atlantic Warm Pool (AWP) comprises the Gulf of Mexico, the Caribbean Sea, and the western tropical North Atlantic. AWP variability occurs on both interannual and multidecadal timescales as well as with a secular variation. The AWP multidecadal variability coincides with the signal of the AMO; that is, the warm (cool) phases of the AMO are characterized by repeated large (small) AWPs. Since the climate response to the North Atlantic SST anomalies is primarily forced at the low latitudes and the AWP is in the path of or a birthplace for Atlantic tropical cyclones, the influence of the AMO on Atlantic tropical cyclone activity may operate through the mechanism of the AWP-induced atmospheric changes. The AWP-induced changes related to tropical cyclones that we emphasize here include a dynamical parameter of tropospheric vertical wind shear and a thermodynamical parameter of convective instability. More specifically, an anomalously large (small) AWP reduces (enhances) the vertical wind shear in the hurricane main development region and increases (decreases) the moist static instability of the troposphere, both of which favor (disfavor) Atlantic tropical cyclone activity. This is the most plausible way in which the AMO relationship with Atlantic tropical cyclones can be understood.

## 1. Introduction

Atlantic tropical cyclone activity has been shown to have largely increased in frequency and intensity since the late 1980s [e.g., *Elsner et al.*, 2000; *Goldenberg et al.*, 2001; *Emanuel*, 2005; *Webster et al.*, 2005]. In particular, the 2005 hurricane season is the most active year on record, with 28 named tropical storms (sustained winds over 18 m/s) in the Atlantic basin and 15 of them reaching hurricane intensity (sustained winds over 33 m/s). The recent increase in Atlantic tropical cyclone activity has fueled a debate on the role of global warming and natural variability of the North Atlantic sea surface temperature (SST) in the increase [e.g., *Goldenberg et al.*, 2001; *Knutson and Tuleya*, 2004; *Emanuel*, 2005; *Webster et al.*, 2005; *Landsea*, 2005; *Zhang and Delworth*, 2006; *Mann and Emanuel*, 2006]. This paper is not meant to resolve the controversy on the relative roles of global warming and natural variability in Atlantic hurricanes. Instead, we mainly focus on the relationships between Atlantic climate variability and Atlantic tropical cyclone activity in a manner that is independent of the ultimate causes of decadal scale changes, and we show why and how Atlantic SST affects Atlantic tropical cyclone activity.

One of the important Atlantic climate phenomena, which influences Atlantic tropical cyclone activity, is the Atlantic Multidecadal Oscillation (AMO) [e.g., *Goldenberg et al.*, 2001; *Bell and Chelliah*, 2006]. The AMO is an oscillatory mode occurring in the North Atlantic SST that operates primarily at the multidecadal timescales of 30-80 years, with its largest variation centered in the high latitudes of the North Atlantic [e.g., *Delworth and Mann,* 2000; *Kerr*, 2000; *Enfield et al.*, 2001]. Recently, a series of papers [*Wang et al.*, 2006; *Wang and Lee*, 2007; *Wang et al.*, 2007, 2008] has been published for pointing out the importance of the Atlantic Warm Pool (AWP) — a large body of warm water comprised of the Gulf of Mexico, the Caribbean Sea, and the western tropical North Atlantic. Since the AWP is in the path of or a

1 birthplace for Atlantic tropical cyclones, it is not surprising that AWP variability affects Atlantic
2 tropical cyclones. The purpose of the present paper is to show that AWP variability contains the
3 multidecadal variability of the AMO, in addition to its interannual and secular variability. We
4 then argue that the influence of the AMO on Atlantic tropical cyclone activity operates through
5 the AWP, which provides a direct effect on the development and intensification of Atlantic
6 tropical cyclones. In other words, the AWP acts as a dynamical and thermodynamical link
7 between the AMO and Atlantic tropical cyclone activity.
8 The remainder of the paper is organized as follows. Section 2 describes the data and
9 model used in this paper. Section 3 discusses global warming mode and the AMO, and section 4
10 shows AWP variability and its link to the AMO. Section 5 shows the relationships of the AWP
11 and AMO with tropospheric vertical wind shear and with Atlantic tropical cyclone activity.
12 Section 6 shows how the atmosphere (i.e., tropospheric vertical wind shear and convective
13 available potential energy) responds to AWP warming/cooling in a numerical model. Finally,
14 section 7 provides a summary.
15
16 **2. Data and Model**
17 Several data sets are used in this study. The first one is an improved extended
18 reconstructed SST (ERSST) data set on a 2° latitude by 2° longitude grid from January 1854 to
19 December 2006 [*Smith and Reynolds*, 2004]. The second data set is the National Centers for
20 Environmental Prediction-National Center for Atmospheric Research (NCEP-NCAR) reanalysis
21 from January 1949 to December 2006 on a 2.5° latitude by 2.5° longitude grid [*Kalnay et al.*,
22 1996]. The variable used in this study is wind velocity at 850 mb and 200 mb. Both of the data
23 sets used here are monthly.

Another data set is the hurricane data based on HURDAT reanalysis database [*Landsea et al.*, 2004], updated to 2006 [*Landsea*, 2007]. The HURDAT reanalysis database attempts to correct systematic and random errors and biases in the original HURDAT data for the period of 1851 to 1910 through historical analyses. *Landsea et al.* [2004] give a detail of the methodologies and references utilized for this reanalysis. What we use in this paper includes the Accumulated Cyclone Energy (ACE), all Atlantic hurricanes (Saffir-Simpson categories 1-5), Atlantic major hurricanes (categories 3-5), and total Atlantic named storms. The ACE index, similar to the Power Dissipation Index (PDI), is one of the most commonly used indices to measure tropical cyclone activity. The ACE index takes into account the number, strength and duration of all tropical cyclones in a season. It is calculated by summing the squares of the estimated maximum sustained velocity of every Atlantic tropical cyclone, at six-hour intervals. The hurricane reanalysis database is available at the website of NOAA/AOML (http://www.aoml.noaa.gov/hrd/data_sub/re_anal.html). Note that hurricane data quality is the subject of intense debate [e.g., *Solow and Moore*, 2002; *Landsea*, 2007; *Chang and Guo*, 2007; *Holland and Webster*, 2007; *Vecchi and Knutson*, 2008]. It is probable that hurricanes were undercounted before the era of aircraft reconnaissance (around the mid-1940s) and satellite technology (the mid-1960s) since hurricanes over the open ocean during that time can be rarely detected. Therefore, we should be cautious of interpreting hurricane data and other data during the early time when measurements are relatively rare.

The atmospheric general circulation model used in this study is the latest version (version 3.1) of the NCAR Community Atmospheric Model (CAM3). The model is a global spectral model with a triangular spectral truncation of the spherical harmonics at zonal wave number 42 (T42), which roughly gives a 2.8° latitude by 2.8° longitude horizontal resolution. It is vertically

divided into 26 hybrid sigma-pressure layers: the upper regions of the atmosphere are gridded by pressure while sigma coordinate system is used for the lower levels and a hybrid coordinate system is used in the middle layers. The CAM3 model is forced by monthly SST from Hadley Centre Sea Ice and SST data set (HadISST) on a 1° latitude by 1° longitude resolution [*Rayner et al.*, 2003].

## 3. Global Warming Mode and the Atlantic Multidecadal Oscillation

An empirical orthogonal function (EOF) analysis is performed on the global annual mean SST over the past 153 years (from 1854 to 2006). The first three EOF modes, which account for 28.3%, 15.3%, and 5.3% of the total variance in the ERSST data, represent global warming, ENSO, and the AMO, respectively. Because the Atlantic sector is the region where our impacts are concentrated and where we wish to describe the relative influences, we compute the variances explained by three modes only in the Atlantic sector which are 23.4%, 7.2% and 10.5%, respectively. The importance of the third mode (the AMO) is greatly increased. We present EOF modes by reconstructing their spatial patterns and time series [*Enfield and Mestas-Nunez*, 1999]. The temporal variation is the spatial average over a reference region of the modal reconstruction of the SST anomalies (unit of °C) rather than the more confusing temporal expansion coefficient (without unit) from which it is derived. The reference region is usually chosen to enclose an area of large spatial amplitude. This is equivalent to multiplying the EOF amplitude time series with the average of its spatial eigenfunction in the reference region. This scaling does not change the character of the time series. The spatial pattern is constructed from the regression coefficient between the reconstructed time series and SST anomalies.

The spatial pattern and temporal reconstruction for the first EOF of the global warming mode are shown in Fig. 1a. For this mode, the obvious reference region to use is over the global ocean. There is warming almost everywhere over the global ocean, with exceptions in the region south of Greenland, in the North and South Pacific, and in the region around Antarctica where cooling occurs. In particular, large warmings occur in the tropical Pacific, Atlantic, and Indian Oceans. The warming pattern in the tropical Pacific is similar to that of the interannual phenomenon of El Niño, with maximum warming in the equatorial eastern Pacific. The basin-wide warming is consistent with expected effects of an increase in greenhouse gas concentrations, and the regional cooling may be suggestive of radiative effects of aerosols or oceanic natural variability [e.g., *Santer et al.*, 2006; *Mann and Emanuel*, 2006; *Hegerl et al.*, 2007]. The temporal variation of Fig. 1a shows a nonlinear and secular increase of SST over the past 153 year. The global ocean has mainly cooled before the 1940s and warmed after the 1940s.

The second EOF mode is ENSO-like, as shown in Fig. 1b. For ENSO-like mode, the reference region is chosen in the Nino3 region (5°N-5°S, 150°W-90°W). The spatial pattern shows a large warming in the equatorial central and eastern Pacific and in the west coastal region from South America to North America. Cooling is displayed in the North and South Pacific Oceans, the Atlantic Ocean, and the Indian Ocean.

The spatial pattern and temporal reconstruction for the third EOF of the AMO mode are shown in Fig. 1c. The reference region of large spatial amplitude is the region of the North Atlantic (40°N-70°N, 60°W-20°W). The spatial pattern shows that the positive SST anomalies are in the North Atlantic, the North Pacific, and the west coast of tropical South America, whereas the negative SST anomalies are located over southern part of all three oceans and in the

equatorial eastern Pacific around 130°W. The Atlantic SST anomalies show a bipolar seesaw pattern [*Stocker*, 1998], supporting the hypothesis that the driving mechanism of the AMO involves fluctuations of the Atlantic meridional overturning circulation [e.g., *Delworth and Mann*, 2000; *Knight et al*., 2005; *Dijkstra et al*., 2006]. As the Atlantic meridional overturning circulation is enhanced, a warming and a cooling will occur in the North and South Atlantic, respectively; and *vice versa* for a reduction of the Atlantic meridional overturning circulation. The time series of Fig. 1c shows that the warm phases of the AMO occur during 1854-1900, 1925-1965, and 1995-2006 and the cool phases are during 1901-1924 and 1966-1994. The AMO is dominated by multidecadal variability.

Apart from the north-south bipolar seesaw, two additional AMO features that contrast with the global warming mode are the strong warming in place of cooling south of Greenland and the lack of strong warming in the Indian Ocean (comparison of Fig. 1a with Fig. 1c). The strong spatial differences between the two modes as well as the contrasting temporal behavior suggest that they arise from fundamentally different processes. This is consistent with the paleoclimate evidence of *Delworth and Mann* [2000] and *Gray et al.* [2004] that AMO-like climate oscillations have existed well before the onset of global warming.

The AMO time series of Fig. 1c is consistent with those of previous studies that define the AMO differently [e.g., *Mestas-Nuñez and Enfield*, 1999; *Enfield et al.*, 2001; *McCabe et al.*, 2004]. *Mestas-Nuñez and Enfield* [1999] use a mode of the rotated EOF analysis as the AMO. *Enfield et al*. [2001] and *McCabe et al*. [2004] define the detrended SST anomalies averaged over the North Atlantic as an AMO index and calculate the correlation of the AMO index with global SST anomalies as AMO spatial pattern. All of these previous studies show a similar AMO index to Fig. 1c. The difference is in the details of AMO spatial patterns, some of which

show a weakly anti-correlated Atlantic SST (or no correlation) between the Northern and Southern Hemispheres. However, this will not affect the results presented in this paper since this paper uses the time series of Fig. 1c (not the spatial pattern) to calculate the AMO relationships with the AWP and Atlantic tropical cyclone activity.

Since global ocean warming is probably not linear, the linear detrended AMO index may still contain the signal of global ocean warming [e.g., *Trenberth and Shea*, 2006; *Mann and Emanuel*, 2006]. Assuming that the AMO does not project onto global ocean warming mode, *Trenberth and Shea* [2006] and *Mann and Emanuel* [2006] remove the global mean SST anomalies from the SST anomalies averaging over the North Atlantic. By doing so, they derive a revised AMO index in which the amplitude of AMO SST anomalies is reduced. Therefore, they conclude that global warming plays an important role in the recent warming in the North Atlantic although the AMO can account for part of the recent warming. Our Figs. 1a and 1c show that the recent warming due to global warming is a little larger than that of the AMO. These results suggest that our approach of defining global warming and the AMO by EOF modes is reasonable and may be a better way.

## 4. Variability of the Atlantic Warm Pool

The Atlantic Warm Pool (AWP) of very warm water is comprised of the Gulf of Mexico, the Caribbean Sea, and the western tropical North Atlantic. Since Atlantic tropical cyclones can be formed in the AWP or be intensified when they pass over AWP warm water [e.g., *Shay et al.*, 2000], it is thus no surprise that AWP variability is important for tropical cyclone activity. Figure 2a shows the June-November (JJASON) AWP area anomaly index which is calculated as the anomalies of the area of SST warmer than 28.5°C divided by the climatological JJASON

AWP area. We focus on the months of JJASON because the official Atlantic hurricane season is from June 1 to November 30. The index displays multiscale variability that includes interannual, multidecadal, and secular variations. The detrended AWP index (subtracting the linear trend from the total area index) is shown in Fig. 2b. To separate longer (mainly multidecadal) from interannual timescale variability, we apply a seven-year running mean to the detrened AWP index (Fig. 2c). Interannual variability is calculated by subtracting the multidecadal variability from the detrended AWP index, as shown in Fig. 2d.

The multidecadal variability (Fig. 2c) shows that the AWPs are large before 1888, during 1934-1962 and after 1995, and small during 1889-1933 and 1963-1994. The periods for large and small AWPs coincide with the warm and cool phases of the AMO (section 3). That is, AWP variability is tied to simultaneous alterations of SST in the high latitudes of the North Atlantic in a mode that operates primarily on the multidecadal timescale.

The interannual phenomenon of ENSO affects the global ocean. The relationship of AWP interannual variability with ENSO over the past 153 years is examined by computing correlations. The correlation between the DJF (December-February) Nino3 SST anomalies and the JJASON AWP interannual index of Fig. 2d is 0.47, suggesting a delayed ENSO effect on the AWP. The delayed impact of ENSO on the AWP has been analyzed by *Enfield et al.* [2006]. However, the contemporaneous correlation of the JJASON Nino3 SST anomalies and JJASON AWP index is only 0.1 (below the 95% significant level). This reflects the fact that (1) large/small AWPs in the summer and fall have no clear relation to contemporaneous El Niño/La Niña development, and (2) by the summer and fall of the following year the Pacific El Niño/ La Niña anomaly has almost always disappeared. These suggest that local processes in the Atlantic

sector play a direct role in the AWP interannual variability, in addition to the remote delayed influence of Pacific ENSO.

As suggested by *Trenberth and Shea* [2006] and *Mann and Emanuel* [2006], a linear detrended analysis may not be a good way for removing global warming since a linear detrended index may still contain the signal of global warming. Here we project the total AWP area index of Fig. 2a onto the first three EOF modes of global warming, ENSO and the AMO by performing a multiple regression. The projected AWP area indices onto global warming, ENSO and the AMO are shown in Figs. 3a-c. As expected, global warming plays an important role in the recent increase of AWP size. However, both the interannual ENSO-like variability and the multidecadal variability of the AMO also contribute to AWP area variation. The phase of the projected AWP onto the AMO is consistent with that of the directly calculated AWP multidecadal area variability (Fig. 2c and Fig. 3c). Apart from the smoothing, the AMO component of AWP variability, defined in this way (Fig. 3c), is similar to that defined by subtraction of a linear trend (Fig. 2c).

Climate variability over the global ocean is intimately linked, possibly through "atmospheric bridges" or teleconnections. Regression coefficients of the global SST anomalies during JJASON onto AWP interannual and multidecadal indices are shown in Figs. 4a and 4b, respectively. On the interannual timescale, warming is found over the tropical North Atlantic, the extratropical North Atlantic, the tropical eastern/central Pacific, and the tropical Indian Ocean, whereas cooling is mainly located in the North and South Pacific. The interannual AWP-related pattern of the global SST anomalies is similar to that of the global nature of ENSO (see Fig. 2 of *Alexander et al.* [2002]), suggesting that the variability is related to the global ocean SST as ENSO signal is. On the multidecadal timescale, a large AWP is associated with a

warming almost everywhere on the global ocean, but with the largest warming in the North Atlantic and the North Pacific. This reflects that the AWP multidecadal variability resembles the AMO (section 3).

Figure 1c shows that when the high latitudes of the North Atlantic are warm, the low latitude regions of the AWP and tropical North Atlantic are also warm. This relation can also be seen by comparing the temporal variation of the AMO (Fig. 1c) with the AWP multidecadal area index (Fig. 2c). The scatter plot of the AMO index and the AWP multidecadal index is shown in Fig. 5. Over the past 153 years, there are 118 years (77%) in which large AWPs occur during the warm phases of the AMO or small AWPs occur during the cool phases of the AMO. Most of the remaining 35 years occur in the warm-to-cool or cool-to-warm transition phases. The warm (cool) phases of the AMO are characterized by repeated large (small) summer/fall AWPs.

It is not surprising that there are more large AWPs when the background SST of the North Atlantic is in warm phases of the multidecadal oscillation. However, since the climate response to the North Atlantic SST anomalies is primarily forced at low latitudes [*Sutton and Hodson*, 2007] and the AWP is in the path of or a birthplace for Atlantic tropical cyclones, it seems plausible that the relationship between the AMO and Atlantic tropical cyclones [*Goldenberg et al.*, 2001] may operate through AWP variability. In section 6, atmospheric general circulation model runs show that a warming in the low latitude region of the AWP alone can decrease the vertical wind shear in the main development region for Atlantic hurricanes, as shown in observations. These suggest that Atlantic hurricane activity is not sensitive to SST variability in the high latitudes of the North Atlantic and low latitude SST plays a key role although the largest SST variability of the AMO is in the high latitudes. In other words, the AWP acts as a link between the AMO and Atlantic hurricane activity.

## 5. Relations to Tropical Cyclones and Vertical Wind Shear

In this section, we first show the variability of Atlantic tropical cyclone activity. We then examine and discuss how Atlantic tropical cyclones vary with the tropospheric vertical wind shear in the main development region (MDR) for Atlantic hurricanes. Finally, we examine the relationships of tropospheric vertical wind shear with the AMO and the AWP.

### 5.1. Atlantic Tropical Cyclone Activity

There is an intense debate regarding hurricane data as they apply to anthropogenic or AMO forcing [e.g., *Solow and Moore*, 2002; *Landsea*, 2007; *Chang and Guo*, 2007; *Holland and Webster*, 2007; *Vecchi and Knutson*, 2008]. It is probable that hurricanes were undercounted before the era of aircraft reconnaissance (around the mid-1940s) and satellite technology (the mid-1960s) since hurricanes over the open ocean during that time were infrequently detected. Many researchers are currently working on this topic. Therefore, we should caution about the hurricane data before the 1940s or the 1960s. Time series of the ACE index, all Atlantic hurricanes, Atlantic major hurricanes and all Atlantic named storms are shown in Fig. 6. Similar to other climate indices, Atlantic tropical cyclone activity also shows a multiscale variability (see Table 1 for the correlations with climate indices). All indices of Atlantic tropical cyclone activity include a multidecadal variation, consistent with the multidecadal variations of the AMO [*Goldenberg et al.*, 2001] and the AWP. Atlantic hurricane seasons since 1995 have been significantly more active than during the previous 25 years. However, the recent increase in Atlantic hurricanes is not unprecedented. The earlier periods of 1945-1970 and 1880-1900 are as active as the most recent decade (Figs. 6a and 6b), and the earlier period of 1900-1940 is as quiet

as the period of 1970-1995. These long-term fluctuations are all consistent with the warm and cool phases of the AMO and AWP, suggesting that the multidecadal variability of oceanic temperatures may be responsible for the multidecadal variation of Atlantic hurricane activity.

As currently being debated, some of the hurricane statistics display trends that may be data-related or at least partially due to global warming. However, for this paper, the important points are that (1) there are contemporaneous multidecadal variations in both the hurricanes and the North Atlantic SST, and (2) the multidecadal SST phases (regardless of their cause) are comprised of lengthy runs of large or small warm pools.

### 5.2. Relationships between Tropical Cyclone Activity and Vertical Wind Shear

The tropospheric vertical wind shear in the MDR (from 10°N-20°N between West Africa and Central America) is believed to be an important factor that affects the formation and development of Atlantic hurricanes [e.g., *Goldenberg and Shapiro*, 1996]. Here we use observational data to show how vertical wind shear varies with tropical cyclones. Following a typical wind shear definition in the literature [e.g., *Goldenberg et al.*, 2001; *Wang et al.*, 2006; *Aiyyer and Thorncroft*, 2006; *Vecchi and Soden*, 2007], we calculate vertical wind shear as the magnitude of the vector difference between winds at 200 mb and 850 mb (i.e., $\left|\vec{V}_{200} - \vec{V}_{850}\right|$). Relationship of vertical wind shear with tropical cyclones is assessed by regressing vertical wind shear onto tropical cyclone indices. Figure 7 shows the regression coefficients of the vertical wind shear during the Atlantic hurricane season of JJASON onto the time series of the ACE, all Atlantic hurricanes, and Atlantic major hurricanes. A common feature is that greater tropical cyclone activity is associated with a negative vertical wind shear anomaly in the MDR, with the maximum wind shear signal in the Caribbean Sea and western tropical North Atlantic. Positive

vertical wind shear is found in the mid-latitudes of the North Atlantic (around 30°N) and the eastern North Pacific. The negative shear in the MDR indicates that a reduction (enhancement) in vertical wind shear is associated with an active (quiet) hurricane season in the Atlantic basin [e.g., *Gray*, 1968; *Pasch and Avila*, 1992; *Goldenberg et al.*, 2001]. Comparison of Figs. 7b and 7c shows that Atlantic major hurricanes correspond to a larger negative change in vertical wind shear, suggesting that large negative wind shear is especially favorable for the intensification of tropical cyclones into major hurricanes.

Another common feature in Fig. 7 is that the negative wind shear regression in the MDR tends towards the northwest to the western Gulf of Mexico and then to the United States and Central America. Since the hurricane data used in Fig. 7 include U.S. landfalling hurricanes, it is suggested that the negative wind shear pattern of Fig. 7 favors a hurricane to be intensified and to make landfall in the United States or Central America. *Wang and Lee* [2008] calculate the regression of the JJASON vertical wind shear onto U.S. landfalling hurricanes (see their Fig. 3) and they clearly show that the negative vertical wind shear in the Caribbean and the western tropical North Atlantic extends toward to the United States via the Gulf of Mexico. This indicates that atmospheric circulation pattern is an important factor for determining whether a hurricane makes landfall in the United States.

### 5.3. Relationships of Vertical Wind Shear with the AMO and the AWP

We first examine how the vertical wind shear in the MDR for Atlantic hurricanes varies. The time series of the vertical wind shear in the MDR during JJASON is shown in Fig. 8, calculating from wind data of the NCEP-NCAR reanalysis from 1949 to 2006. The vertical wind shear shows a multiscale variability that includes secular, multidecadal, and interannual

timescale variations. The wind shear indices are significantly correlated with Atlantic tropical cyclone activity (Table 1). Again, we project the total vertical wind shear of Fig. 8a onto the first three EOF modes of global warming, ENSO and the AMO (Fig. 9). The amplitude of the vertical wind shear projected onto the AMO is much larger than that of global warming (Figs. 9a and 9c). Both the linear trend wind shear and the wind shear projected onto global warming mode show a secular increase of vertical wind shear since 1949 (Figs. 8a and 9a). The vertical wind shear projected onto AMO explains a large portion of the total vertical wind shear signal, whereas the wind shear projected onto the interannual ENSO-like variability is very small (Fig. 9b). The vertical wind shear projected onto the AMO shows a similar phase to the multidecadal vertical wind shear directly calculated (Figs. 8c and 9c).

The secular increase of vertical wind shear suggests that global warming may disfavor Atlantic hurricane activity, consistent with the result of future model projections under global warming scenarios for the 21$^{st}$ century [*Vecchi and Soden,* 2007]. However, we should keep in mind that the vertical wind shear is not the only factor affecting Atlantic hurricane activity. Other factors, such as the direct effect of increasing Atlantic SST on potential intensity, may be offsetting the impact of the increasing shear leading to some increase in storm activity [e.g., *Emanuel*, 2005]. Currently, we are uncertain about what the net effect of these offsetting influences is. Figures 8c and 9c show greater wind shear during 1970-1993 and weaker wind shear before and after. This is closely tied to the multidecadal variations of the AWP (Fig. 2c), the AMO (Fig. 1c), and tropical cyclone indices (Fig. 6). The consistent relationship among ocean temperature, wind shear and tropical cyclones, which are derived from independent data sets, offers support to their veracity. It also suggests that the multidecadal variability is a robust

feature as also evidenced by a tree ring proxy dating to the 16th century [*Gray et al.*, 2004], and that Atlantic tropical cyclone activity does vary with a slow change in Atlantic SST.

How does vertical wind shear vary with the AWP multidecadal and interannual variations? To answer this question, we first normalize the AWP indices in Figs. 2b-d and then regress the JJASON vertical wind shear onto these normalized AWP indices (Fig. 10). The AWP is associated with negative wind shear regressions in the MDR and positive wind shear in the eastern North Pacific (Fig. 10a). This is very similar to the activity-shear relationship seen in Fig. 7. These features are consistent with the numerical modeling result (next section) that anomalously large (small) AWPs weaken (strengthen) the vertical wind shear in the MDR and strengthen (weaken) the vertical wind shear in the eastern North Pacific. Both the AWP multidecadal and interannual variability contribute to the wind shear distribution. However, there is a difference between the AWP-induced multidecadal and interannual wind shears. First, the AWP multidecadal variability is associated with the wind shear in the central tropical North Atlantic, whereas the AWP interannual variability corresponds to the wind shear in the Caribbean Sea and the western tropical North Atlantic. Second, the AWP-induced wind shear on the multidecadal timescale is larger than that on the interannual timescale, consistent with the fact that Atlantic tropical cyclone activity follows more closely the AWP multidecadal variability (see Table 1).

As shown in previous sections, the AMO is dominated by multidecadal variability. Regression of the JJASON vertical wind shear onto the AMO index is shown in Fig. 11a. As expected, the wind shear regression pattern in the tropical North Atlantic is similar to that of the AWP multidecadal variability. However, unlike the AWP, the AMO shows a negative regression in the eastern North Pacific (compare Fig. 10a with Fig. 11a). ENSO-induced wind

shear pattern during JJASON (Fig. 11b) is opposite to that of the AWP interannual variability (Fig. 10c). A positive wind shear is located in the Caribbean, whereas the negative wind shear is in the eastern North Pacific. This indicates that El Niño (La Niña) is associated with a strong (weak) wind shear in the Caribbean and a weak (strong) wind shear in the eastern North Pacific. This El Niño (La Niña) wind shear pattern thus disfavors (favors) tropical cyclones in the Atlantic basin and favors (disfavors) tropical cyclones in the eastern North Pacific. The zonal displacement of the shear signal in the Atlantic and the opposite behavior in the eastern North Pacific are features that distinguish the interannual and multidecadal relationships amongst the AWP, shear and tropical cyclone activity and are indicative of differences in the way the atmosphere responds to ENSO and the AWP.

## 6. Atmospheric Model Responses to AWP SST

Sections 3 and 4 show that the warm (cool) phases of the AMO are populated by more frequently large (small) AWPs and their relationships to the vertical shear and TC activity are similar. *Wang and Lee* [2007], and *Wang et al.* [2007, 2008] have demonstrated that both the annual and anomalous AWPs can reduce the tropospheric vertical wind shear in the MDR and increase the moist static instability of the troposphere, both of which favor hurricane development. In this section, we will briefly summarize and discuss how the AWP SST causes atmospheric changes in the CAM3 model that are related to Atlantic tropical cyclone activity.

We present two sets of ensemble model simulations: large AWP (LAWP) and small AWP (SAWP). In the LAWP run, the CAM3 model is forced by the twelve-monthly SSTs for the large AWP composites in the AWP region (from 5°N to 30°N between 40°W and the coast of the Americas), while the monthly HadISST climatology is specified for the rest of the global

ocean. In the set of the SAWP simulation, the CAM3 model is forced by the small AWP monthly SST composites in the AWP region and climatological SST elsewhere. For each set of simulations the model is integrated for 20 years. The first two years of output are discarded to exclude any possible transient spin up effects. A time mean is then calculated by averaging together the output for the remaining 18 years over the six-month period of JJASON. Assuming that each year is statistically independent, this is equivalent to an ensemble mean with 18 members. To clearly examine the effect of the anomalous AWP, the difference is taken between the LAWP and SAWP runs (LAWP minus SAWP). We note that because of the non-linear Clausius-Clapyron relationship, virtually all of the atmospheric heating occurs at higher SSTs, which also outlines the region where hurricanes develop. There is less evidence that incipient easterly waves coming off West Africa are affected by SST anomalies at the lower absolute temperatures found east of about 50°W. Thus, the LAWP and SAWP model experiments are good schemes that disproportionately weight the influence of SST anomalies at the higher absolute temperatures of the AWP region.

The atmospheric circulation responses to LAWP – SAWP are shown in Fig. 12. Consistent with *Gill*'s [1980] dynamics, the atmospheric response to the AWP's heating is baroclinic. The lower troposphere shows a cyclonic circulation in the AWP and eastern North Pacific (Fig. 12b), whereas the upper troposphere has an anticyclonic circulation pattern (Fig. 12a). In the tropical North Atlantic, the mean circulation features the easterly trade winds in the lower troposphere and the westerly winds in the upper troposphere. Thus, the AWP-induced cyclonic and anticyclonic anomalous circulation patterns reduce both the lower tropospheric easterly winds and the upper tropospheric westerly winds, resulting in a reduction of the vertical wind shear in the MDR (Fig. 12c). In the eastern North Pacific, the mean zonal circulation is

relatively weak, owing to the presence of the eastern Pacific intertropical convergence zone (ITCZ). The AWP-induced baroclinic wind patterns in the eastern North Pacific in Fig. 12 thus increase the vertical wind shear there, in agreement with observations (Fig. 10a). This suggests that a large (small) AWP favors (disfavors) Atlantic tropical cyclones, whereas a large (small) AWP suppresses (enhances) tropical cyclones in the eastern Pacific.

We note that the large-scale circulation anomalies associated with ENSO are quite distinct from Fig. 12 (not shown) although they do result in the shear signal in the Caribbean. In particular, the juxtaposed baroclinic circulation anomalies centered north of the Caribbean are lacking in the ENSO response, and the ENSO shear signal is dominated by the upper troposphere winds.

Convective Available Potential Energy (CAPE), which is a measure of the moist static instability of the troposphere, represents the amount of buoyant energy available to accelerate a parcel vertically, or the amount of work a parcel does on the environment. CAPE is especially important when air parcels are able to reach the layer of free convection. The higher the CAPE value, the more energy available to foster storm growth (or for an easterly wave to become a tropical storm). CAPE provides the fuel for moist convection, thus it also is a potential indicator of hurricane intensity [*Emanuel*, 1994]. Figure 13 shows that the model's CAPE response to LAWP – SAWP forcing during JJASON is a large positive value in the tropical North Atlantic. That is, an anomalously large (small) AWP tends to increase (decrease) CAPE due to the increased (decreased) near-surface air temperature and water vapor content and the dynamic uplift associated with the cyclonic circulation anomaly at low levels (Fig. 12b), which increases the relative humidity. The positive CAPE anomaly in Fig. 13 is orientated in the direction of southeast-to-northwest. The southeast-to-northwest orientation lies along the track of many

historical storms with disastrous landfall in the United States that typically develop from easterly waves off Africa during August-September. This suggests that the AWP may play a role in the hurricane track.

Significantly, the effect of the AWP on CAPE reinforces the effect on shear, vis-à-vis hurricane activity. In contrast, composite mean distributions based on the NCEP-NCAR reanalysis show that the ENSO impact on tropical Atlantic CAPE is opposite to that of the shear (not shown). This is yet another indication of the differences between the tropospheric responses to ENSO and the AWP, and helps to explain why the empirical linkage between the AMO/AWP and hurricane activity is stronger than the ENSO relationship.

## 7. Summary

In this paper we provide evidence that the Atlantic Warm Pool (AWP) and its effects on tropospheric vertical shear and moist static instability are most likely responsible for the relationship, shown by *Goldenberg et al*. [2001], between the Atlantic Multidecadal Oscillation (AMO) and Atlantic hurricane activity. Our model runs show that an SST warming in the low latitudes of the AWP region alone can decrease the tropospheric vertical wind shear in the main development region (MDR) for Atlantic hurricanes, in agreement with observations. The analyses of the long-term SST data in sections 3 and 4 show that the multidecadal signal of the AMO includes more repeated appearance of large summer warm pools. All of these suggest that the relationship between the AMO and Atlantic tropical cyclones may operate through AWP variability. In other words, the AWP acts as a link between the AMO and Atlantic tropical cyclones, providing a direct influence on atmospheric dynamical and thermodynamical variables in the MDR.

The AWP can affect the dynamical parameter of the vertical wind shear and the thermodynamical parameter of the moist static instability in the MDR that in turn influence Atlantic tropical cyclone activity. Dynamically, the AWP-induced atmospheric circulation pattern is baroclinic [*Gill*, 1980], with a cyclone in the lower troposphere and an anticyclone in the upper troposphere. This circulation structure reduces the lower tropospheric easterly and the upper tropospheric westerly, resulting in a reduction of the vertical wind shear that favors atmospheric convection. Thermodynamically, the AWP increases CAPE that provides the fuel for moist convection and thus facilitates the formation and development of Atlantic tropical cyclones.

**Acknowledgments**

We thank comments and suggestions provided by Drs. Michael Mann and Jay Gulledge and two other anonymous reviewers. This work was supported by a grant from National Oceanic and Atmospheric Administration (NOAA) Climate Program Office and by the base funding of NOAA Atlantic Oceanographic and Meteorological Laboratory (AOML). The findings and conclusions in this report are those of the author(s) and do not necessarily represent the views of the funding agency.

## References


Aiyyer, A. R., and C. Thorncroft (2006), Climatology of vertical wind shear over the tropical Atlantic, *J. Clim. 19*, 2969-2983

Alexander, M. A., et al. (2002), The atmospheric bridge: The influence of ENSO teleconnections on air-sea interaction over the global oceans, *J. Clim.*, *15*, 2205-2231.

Bell, G. D., and M. Chelliah (2006), Leading tropical modes associated with interannual and multidecadal fluctuations in north Atlantic hurricane activity, *J. Clim., 19*, 590-612.

Chang, E. K. M., and Y. Guo (2007), Is the number of North Atlantic tropical cyclones significantly underestimated prior to the availability of satellite observations? *Geophys. Res. Lett., 34*, L14801, doi:10.1029/2007GL030169.

Delworth, T. L., and M. E. Mann (2000), Observed and simulated multidecadal variability in the Northern Hemisphere, *Clim. Dyn., 16*, 661-676.

Dijkstra, H. A., L. te Raa, M. Schmeits, and J. Gerrits (2006), On the physics of the Atlantic multidecadal oscillation, *Ocean Dyn., 56*, 36-50.

Elsner, J. B., T. Jagger, and X.-F. Liu (2000), Changes in the rates of North Atlantic major hurricane activity during the 20th century, *Geophys. Res. Lett., 27*, 1743-1746.

Emanuel, K. A. (1994), *Atmospheric Convection*, Oxford Univ. Press, New York, 580 pp.

Emanuel, K. (2005), Increasing destructiveness of tropical cyclones over the past 30 years, *Nature, 436*, 686-688.

Enfield, D. B., and A. M. Mestas-Nunez (1999), Multiscale variabilities on global sea surface temperatures and their relationships with tropospheric climate patterns, *J. Clim., 12*, 2719-2733.

Enfield, D. B., A. M. Mestas-Nunez, and P. J. Trimble (2001), The Atlantic multidecadal oscillation and its relationship to rainfall and river flows in the continental US, *Geophys. Res. Lett.*, *28*, 2077-2080.

Enfield, D. B., S.-K. Lee, and C. Wang (2006), How are large Western Hemisphere warm pools formed, *Prog. Oceanogr.*, *70*, 346-365.

Gill, A. E. (1980), Some simple solutions for heat-induced tropical circulation, *Quart. J. Roy. Meteor. Soc.*, *106*, 447-462.

Goldenberg, S. B., and L. J. Shapiro (1996), Physical mechanisms for the association of El Niño and West African rainfall with Atlantic major hurricane activity, *J. Clim., 9*, 1169-1187.

Goldenberg, S. B., C. W. Landsea, A. M. Maestas-Nunez, and W. M. Gray (2001), The recent increase in Atlantic hurricane activity: Causes and implications, *Science, 293*, 474-479.

Gray, W. M. (1968), Global view of the origin of tropical disturbances and storms, *Mon. Weather Rev.*, *96*, 669-700.

Gray, S. T., J. L. Graumlich, J. L. Betancourt, and G. T. Pederson (2004), A tree-ring based reconstruction of the Atlantic Multidecadal Oscillation since 1567 A.D., *Geophys. Res. Lett., 31*, L12205, doi:10.1029/2004GL019932.

Holland, G. J., and P. J. Webster (2007), Heightened tropical cyclone activity in the North Atlantic: natural variability or climate trend? *Phil. Trans. R. Soc. A* doi:10.1098/rsta.2007.2083.

Hegerl, G. C. et al. (2007): Understanding and Attributing Climate Change. In: *Climate Change 2007: The Physical Science Basis. Contribution of Working Group I to the Fourth Assessment Report of the Intergovernmental Panel on Climate Change,* edited by S.

Solomon et al., Cambridge University Press, Cambridge, United Kingdom and New York, NY, USA.

Kalnay, E. et al. (1996), The NCEP/NCAR 40-year reanalysis project, *Bull. Am. Meteorol. Soc.*, *77*, 437-471.

Kerr, R. A. (2000), A North Atlantic climate pacemaker for the centuries, *Science, 288*, 1984-1986.

Knight, J. R. et al. (2005), A signature of persistent natural thermohaline circulation cycles in observed climate, *Geophys. Res. Lett., 32*, doi:10.1029/2005GL024233.

Knutson, T. R., and R. E. Tuleya (2004), Impact of $CO_2$-induced warming on simulated hurricane intensity and precipitation: Sensitivity to the choice of climate model and convective parameterization, *J. Clim., 17*, 3477-3495.

Landsea, C. W. et al. (2004), The Atlantic hurricane database re-analysis project: Documentation for the 1851-1910 alterations and additions to the HURDAT database, in *Hurricanes and Typhoons: Past, Present and Future,* edited by R. J. Murnane and K.-B. Liu, pp. 177-221, Columbia Univ. Press, New York.

Landsea, C. W. (2005), Hurricanes and global warming, *Nature, 438*, E11-E13.

Landsea, C. W. (2007), Counting Atlantic tropical cyclones back to 1900, *Eos Tans. AGU, 88*, 197-208, doi:10.1029/2007EO180001.

Mann, M. E., and K. A. Emanuel (2006), Atlantic hurricane trends linked to climate change, *Eos Trans. AGU*, *87*, 233-244, doi:10.1029/2006EO240001.

McCabe, G., M. Palecki, and J. Betancourt (2004), Pacific and Atlantic Ocean influences on multidecadal drought frequency in the United States, *Proc. Nat. Acad. Sci.*, *101*, 4136-4141.

Mestas-Nunez, A. M., and D. B. Enfield (1999), Rotated global modes of non-ENSO sea surface temperature variability, *J. Clim., 12*, 2734-2746.

Pasch, R. J., and L. A. Avila (1992), Atlantic hurricane seasons of 1991, *Mon. Wea. Rev.*, *120*, 2671-2687.

Rayner, N. A. et al. (2003), Global analysis of sea surface temperature, sea ice and night marine air temperature since the late nineteenth century, *J. Geophys. Res.*, *108*, 4407, doi:10.1029/2002JD002670.

Santer, B. D. et al (2006), Forced and unforced ocean temperature changes in Atlantic and Pacific tropical cyclogenesis regions, *Proc. Nat. Acad. Sci., 203*, 13905-13910.

Shay, L. K., G. J. Goni, and P. G. Black (2000), Effects of a warm oceanic feature on Hurricane Opal, *Mon. Wea. Rev.*, *128*, 1366-1383.

Smith, T. M., and & R. W. Reynolds (2004), Improved extended reconstruction of SST (1854-1997), *J. Clim.*, *17*, 2466-2477.

Solow, A. R., and L. J. Moore (2002), Testing for trend in North Atlantic hurricane activity, 1900-98, *J. Clim., 15*, 3111-3114.

Stocker, T. F. (1998), The seesaw effect, *Science, 282*, 61-62.

Sutton, R. T., and D. L. R. Hodson (2007), Climate response to basin-scale warming and cooling of the North Atlantic Ocean, *J. Clim.*, *20*, 891-907.

Trenberth, K.E., and D.J. Shea (2006), Atlantic hurricanes and natural variability in 2005, *Geophys. Res. Lett., 33*, L12704, doi:10.1029/2006GL026894.

Vecchi, G. A., and B. J. Soden (2007), Increased tropical Atlantic wind shear in model projections of global warming, *Geophys. Res. Lett., 34*, 10.1029/2006GL028905.

Vecchi, G. A., and T. R. Knutson (2008), On estimates of historical North Atlantic tropical cyclone activity, *J. Clim.*, in press.

Wang, C., D. B. Enfield, S.-K. Lee, and C. W. Landsea (2006), Influences of the Atlantic warm pool on Western Hemisphere summer rainfall and Atlantic hurricanes, *J. Clim.*, *19*, 3011-3028.

Wang, C., and S.-K. Lee (2007), Atlantic warm pool, Caribbean low-level jet, and their potential impact on Atlantic hurricanes, *Geophys. Res. Lett.*, *34*, doi:10.1029/2006GL0028579.

Wang, C., and S.-K. Lee (2008), Global warming and United States landfalling hurricanes, *Geophys. Res. Lett.*, *35*, L02708, doi:10.1029/2007GL032396.

Wang, C., S.-K. Lee, and D. B. Enfield (2007), Impact of the Atlantic warm pool on the summer climate of the Western Hemisphere, *J. Clim.*, *20*, 5021-5040.

Wang, C., S.-K. Lee, and D. B. Enfield (2008), Climate response to anomalously large and small Atlantic warm pools during the summer, *J. Clim.*, in press.

Webster, P. J., G. J. Holland, J. A. Curry, and H.-R. Chang (2005), Changes in tropical cyclone number, duration, and intensity in a warming environment, *Science, 309*, 1844-1846.

Zhang, R., and T. L. Delworth (2006), Impact of Atlantic multidecadal oscillation on India/Sahel rainfall and Atlantic hurricanes, *Geophys. Res. Lett.*, *33*, doi:10.1029/2006GL026267.

## Figure Captions

**Figure 1.** The first three empirical orthogonal function (EOF) modes, representing (a) global warming mode (top two panels), (b) ENSO-like mode (middle two panels) and (c) the AMO (bottom two panels). The EOF modes are presented by reconstructing their spatial patterns and expansion coefficients of time series. The temporal variations are the spatial average over the reference regions of (a) the global ocean, (b) the Nino3 region (5°N-5°S, 150°W-90°W), and (c) the North Atlantic (40°N-70°N, 60°W-20°W) of the modal reconstruction of SST (in unit of °C) rather than the more confusing temporal amplitude (without unit) from which it is derived. This is equivalent to multiplying the EOF time series with the average of their spatial eigenfunctions over the reference regions. This scaling does not change the character of the time series. The spatial patterns are constructed from the regression coefficients (°C per °C) between the reconstructed time series and SST anomalies.

**Figure 2**. AWP area anomaly indices (%) during the Atlantic hurricane season of June-November (JJASON). The area index is calculated as the anomalies of the area of SST warmer than 28.5°C divided by the climatological JJASON AWP area. Shown are the (a) total, (b) detrended (removing the linear trend), (c) multidecadal, and (d) interannual area anomalies. The multidecadal variability is obtained by performing a seven-year running mean to the detrened AWP index. The interannual variability is calculated by subtracting the multidecadal variability from the detrended AWP index. The multidecadal (interannual) variability accounts for 54% (46%) of the total variance of the detrended AWP index. The black straight line in (a) is the linear trend that is fitted to the total area anomaly.

**Figure 3.** The projections of the total AWP area index of Fig. 2a onto (a) global warming mode, (b) ENSO-like variation and (c) the AMO.

**Figure 4.** Regression coefficients (°C per 100%) of the global SST anomalies during JJASON onto the AWP (a) interannual and (b) multidecadal area indices in Fig. 2.

**Figure 5**. The scatter plot of the AMO index versus the AWP multidecadal index. Blue dot indicates that the AWP is positively related to the AWP, whereas red plus means that the AMO is negatively correlated with the AWP.

**Figure 6.** Time series of (a) the ACE ($10^4$ $kt^2$), (b) the number of all Atlantic hurricanes (Categories 1-5), (c) the number of Atlantic major hurricanes (Categories 3-5), and (d) all Atlantic named storms. The black straight line represents the mean value from 1851 to 2006. The blue line is the seven-year running mean, emphasizing longer (than interannual) timescale variations.

**Figure 7.** Regression coefficients of the vertical wind shear during JJASON onto (a) the ACE, (b) all Atlantic hurricanes, and (c) Atlantic major hurricanes.

**Figure 8**. Time series of the vertical wind shear in the MDR (85°W-15°W, 10°N-20°N) for Atlantic hurricanes during JJASON. The vertical wind shear is calculated as the magnitude of the vector difference between winds at 200 mb and 850 mb. Shown are the (a) total, (b)

detrended (removing the linear trend), (c) multidecadal, and (d) interannual variations. The multidecadal variability is obtained by performing a seven-year running mean to the detrened wind shear. The interannual variability is calculated by subtracting the multidecadal variability from the detrended wind shear. The black straight line in (a) is the linear trend that is fitted to the total wind shear.

**Figure 9.** The projections of the vertical wind shear of Fig. 8a onto (a) global warming mode, (b) ENSO-like variation and (c) the AMO.

**Figure 10.** Regressions of the vertical wind shear during JJASON onto the AWP (a) detrended, (b) multidecadal, and (c) interannual indices. The AWP detrended, multidecadal, and interannual area indices in Figs. 2b-d are first normalized by their maxima. Then the regressions are calculated.

**Figure 11.** Regression coefficients of the vertical wind shear during JJASON onto (a) the AMO index and (b) the JJASON Nino3 SST anomalies.

**Figure 12.** Atmospheric response to the LAWP and SAWP model ensemble runs (LAWP – SAWP) during June-November (JJASON). Shown are (a) geopotential height ($10^2$ m) and wind (m $s^{-1}$) at 200 mb, (b) geopotential height and wind at 850 mb, and (c) vertical wind shear (m $s^{-1}$) between 200 mb and 850 mb.

**Figure 13.** Response of Convective Available Potential Energy (CAPE; J/kg) to the LAWP and SAWP model ensemble runs (LAWP – SAWP) during June-November (JJASON).

**Table 1.** Correlations of various indices with the Accumulated Cyclone Energy (ACE) index, all Atlantic hurricanes, Atlantic major hurricanes, and total Atlantic named storms. Tropical cyclone data is from 1851-2006 and the ERSST is from 1854-2006. The vertical wind shear (VWS) of the NCEP-NCAR reanalysis is from 1949-2006. The correlation above the 95% significant level is in bold.

| | ACE | All hurricanes | Major hurricanes | All storms |
|---|---|---|---|---|
| Global warming mode | 0.07 | **0.18** | 0.10 | **0.28** |
| ENSO-like mode | **-0.38** | **-0.42** | **-0.42** | **-0.44** |
| AMO mode | **0.26** | **0.22** | 0.14 | 0.12 |
| AWP (total) | **0.36** | **0.43** | **0.37** | **0.51** |
| AWP (multidecadal) | **0.25** | **0.32** | **0.28** | **0.43** |
| AWP (interannual) | **0.16** | **0.18** | 0.13 | **0.18** |
| VWS (total) | **-0.61** | **-0.52** | **-0.59** | **-0.41** |
| VWS (multidecadal) | **-0.37** | -0.19 | **-0.39** | -0.05 |
| VWS (interannual) | **-0.44** | **-0.44** | **-0.39** | **-0.40** |

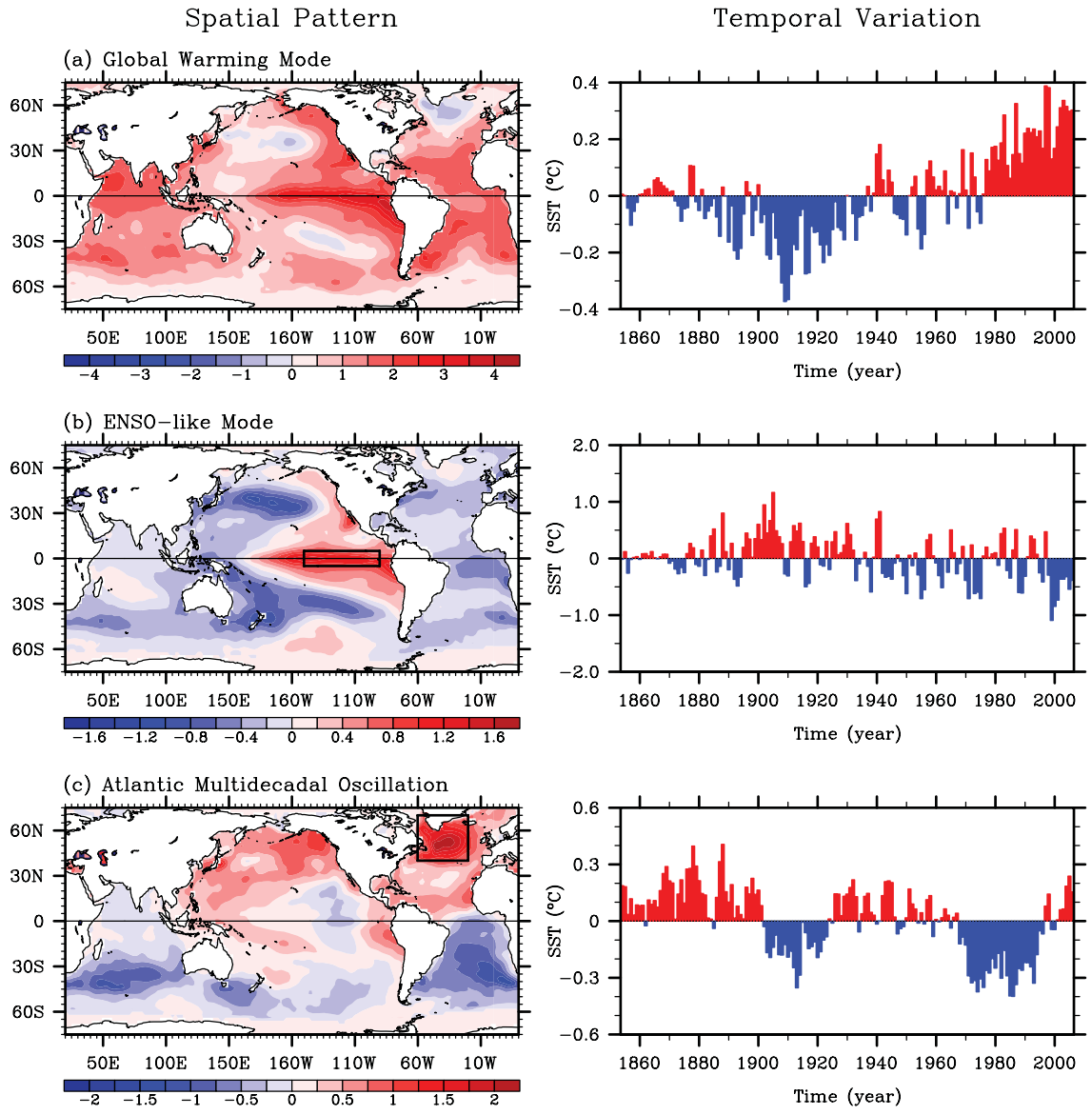


**Figure 1.** The first three empirical orthogonal function (EOF) modes, representing (a) global warming mode (top two panels), (b) ENSO-like mode (middle two panels) and (c) the AMO (bottom two panels). The EOF modes are presented by reconstructing their spatial patterns and expansion coefficients of time series. The temporal variations are the spatial average over the reference regions of (a) the global ocean, (b) the Nino3 region (5°N-5°S, 150°W-90°W), and (c) the North Atlantic (40°N-70°N, 60°W-20°W) of the modal reconstruction of SST (in unit of °C) rather than the more confusing temporal amplitude (without unit) from which it is derived. This is equivalent to multiplying the EOF time series with the average of their spatial eigenfunctions over the reference regions. This scaling does not change the character of the time series. The spatial patterns are constructed from the regression coefficients (°C per °C) between the reconstructed time series and SST anomalies.

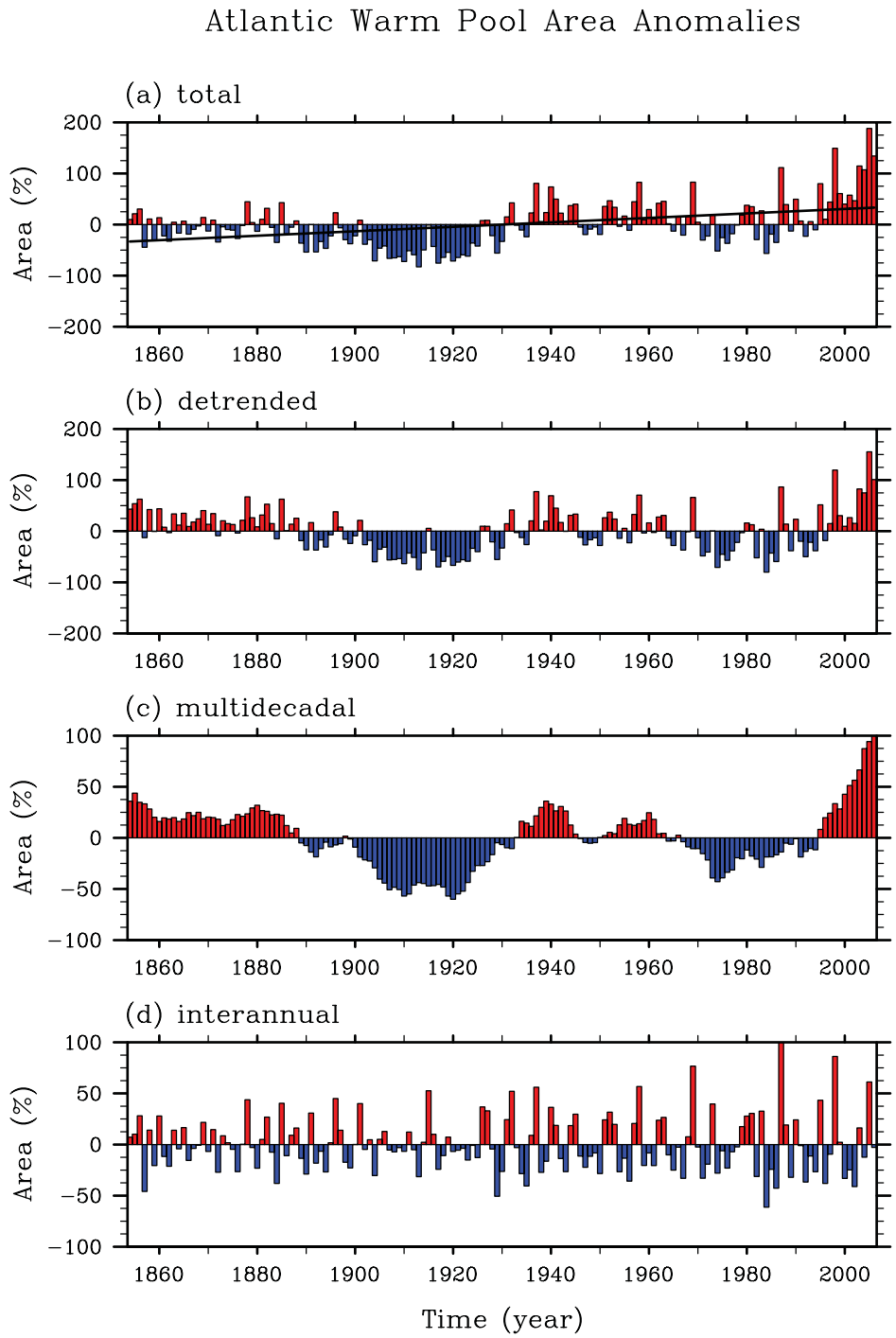


**Figure 2**. AWP area anomaly indices (%) during the Atlantic hurricane season of June-November (JJASON). The area index is calculated as the anomalies of the area of SST warmer than 28.5°C divided by the climatological JJASON AWP area. Shown are the (a) total, (b) detrended (removing the linear trend), (c) multidecadal, and (d) interannual area anomalies. The multidecadal variability is obtained by performing a seven-year running mean to the detrened AWP index. The interannual variability is calculated by subtracting the multidecadal variability from the detrended AWP index. The multidecadal (interannual) variability accounts for 54% (46%) of the total variance of the detrended AWP index. The black straight line in (a) is the linear trend that is fitted to the total area anomaly.

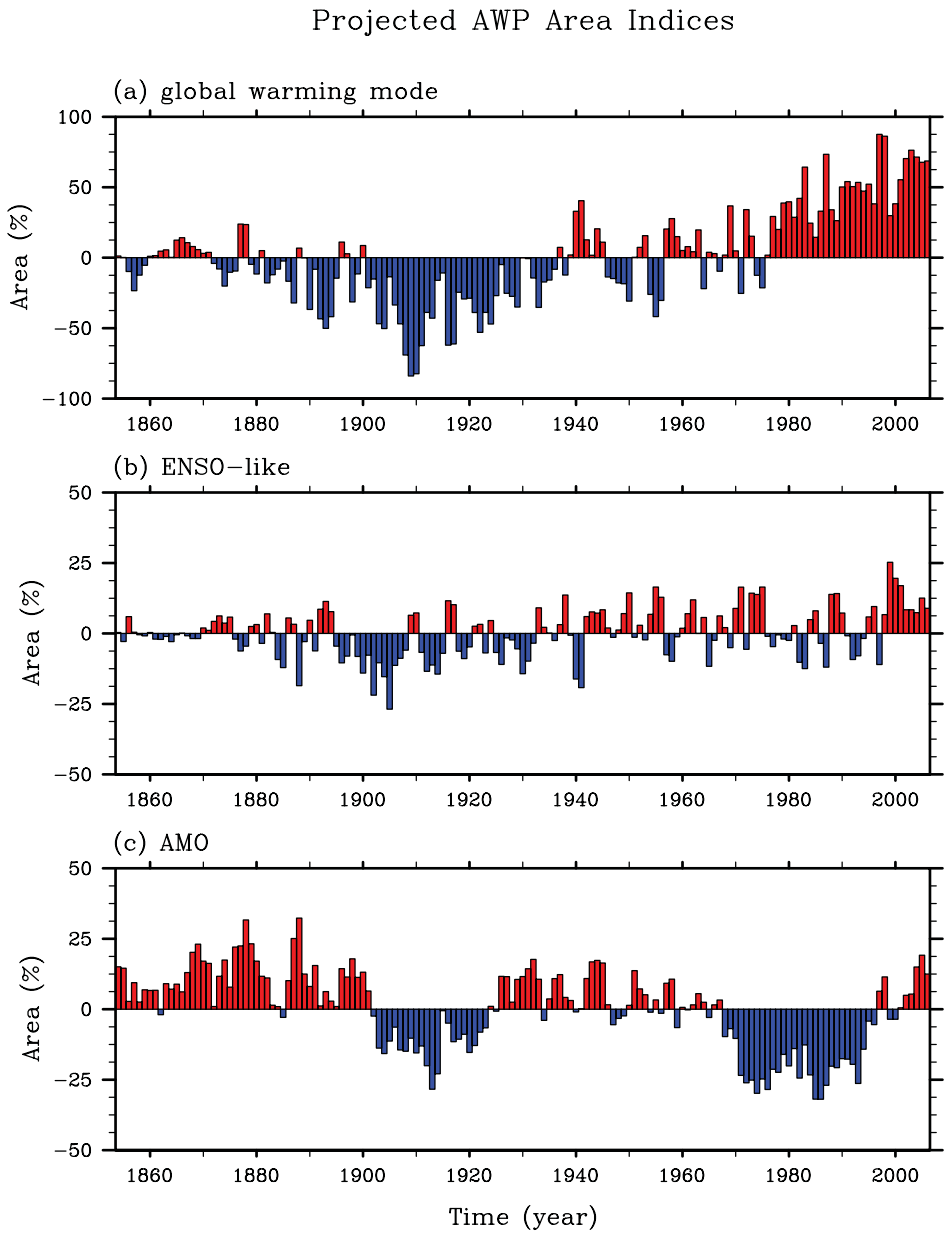


**Figure 3.** The projections of the total AWP area index of Fig. 2a onto (a) global warming mode, (b) ENSO-like variation and (c) the AMO.

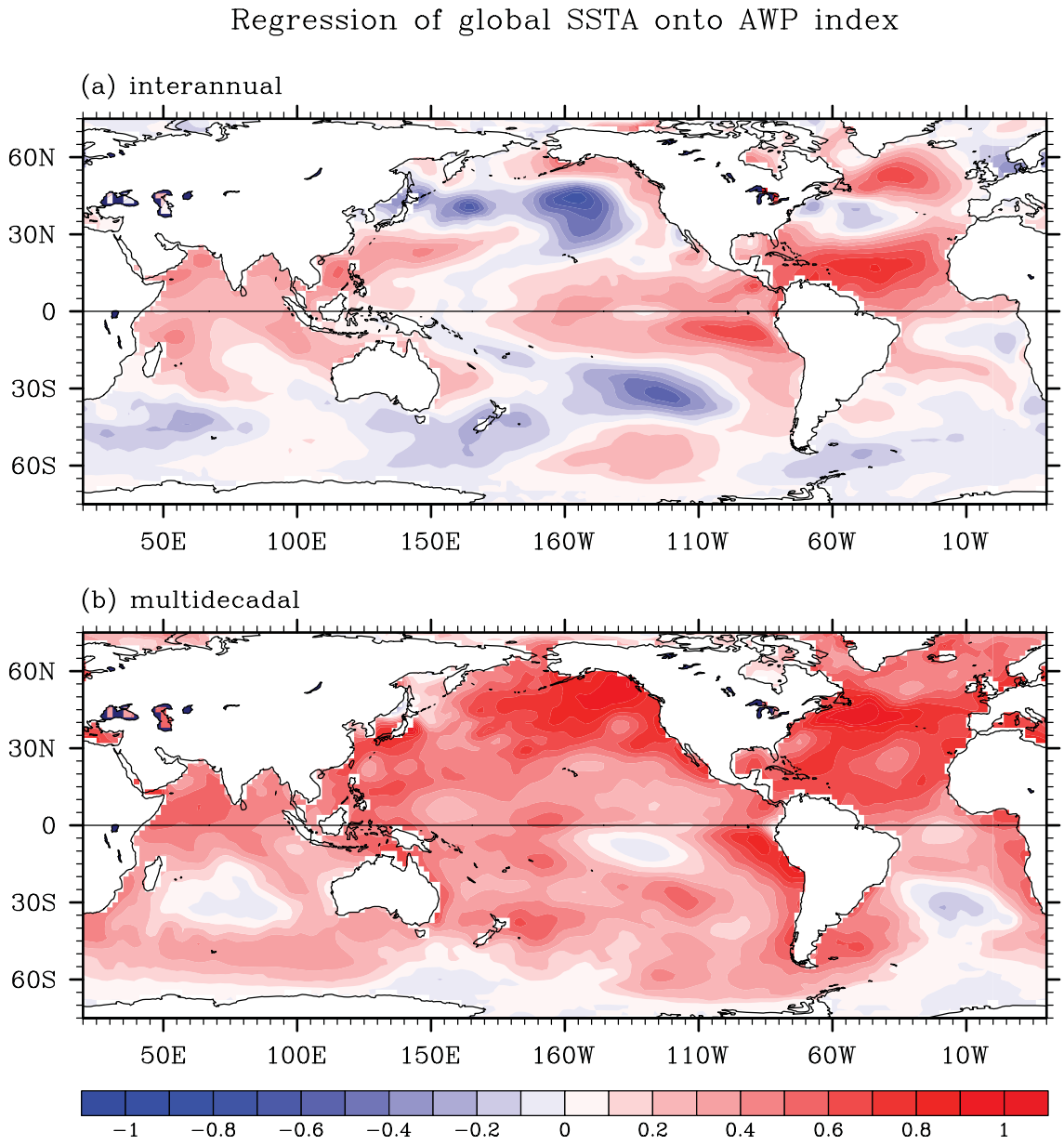


**Figure 4.** Regression coefficients (°C per 100%) of the global SST anomalies during JJASON onto the AWP (a) interannual and (b) multidecadal area indices in Fig. 2.

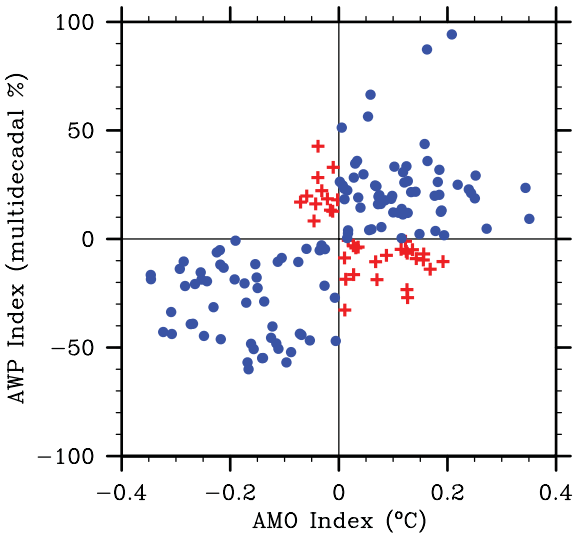


**Figure 5**. The scatter plot of the AMO index versus the AWP multidecadal index. Blue dot indicates that the AWP is positively related to the AWP, whereas red plus means that the AMO is negatively correlated with the AWP.

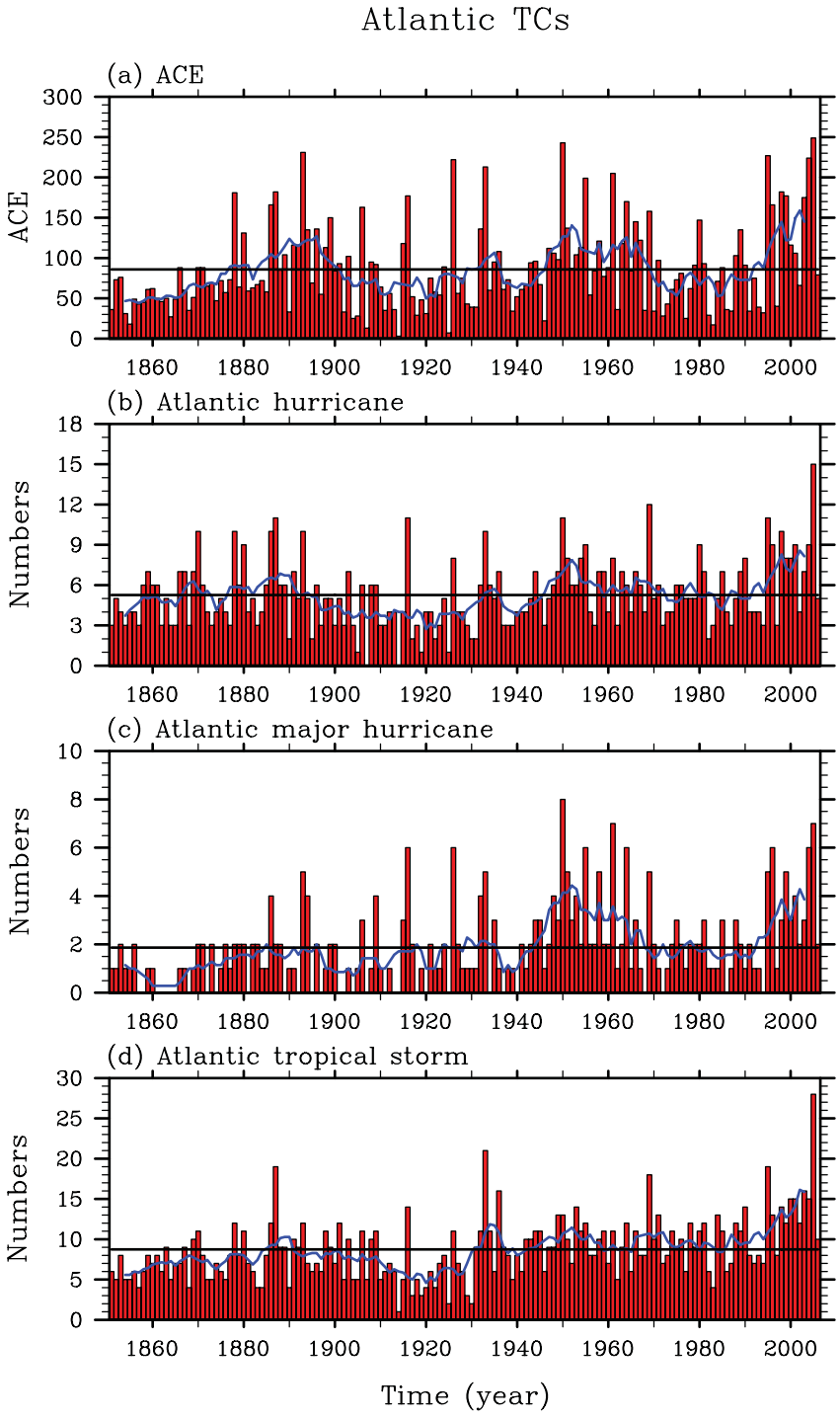


**Figure 6.** Time series of (a) the ACE ($10^4$ $kt^2$), (b) the number of all Atlantic hurricanes (Categories 1-5), (c) the number of Atlantic major hurricanes (Categories 3-5), and (d) all Atlantic named storms. The black straight line represents the mean value from 1851 to 2006. The blue line is the seven-year running mean, emphasizing longer (than interannual) timescale variations.

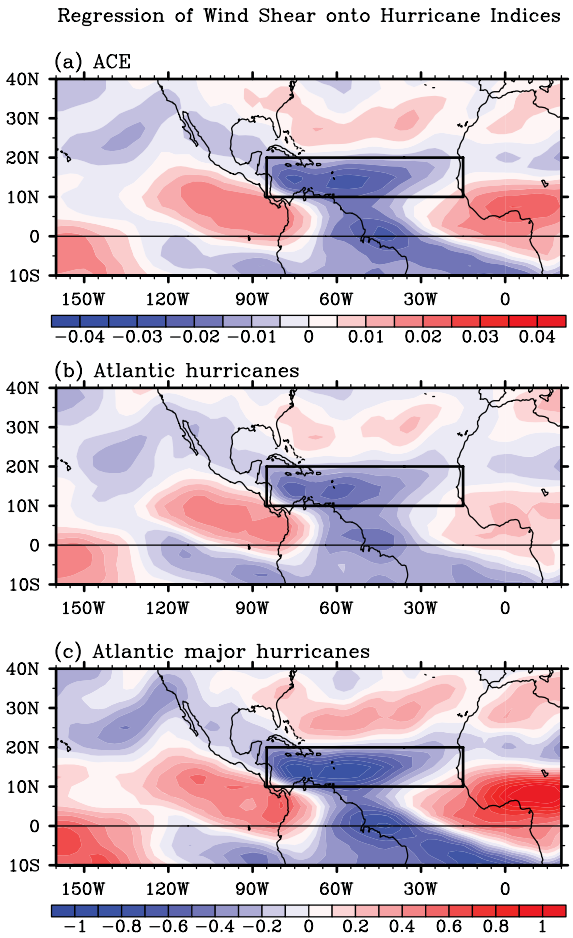


**Figure 7.** Regression coefficients of the vertical wind shear during JJASON onto (a) the ACE, (b) all Atlantic hurricanes, and (c) Atlantic major hurricanes.

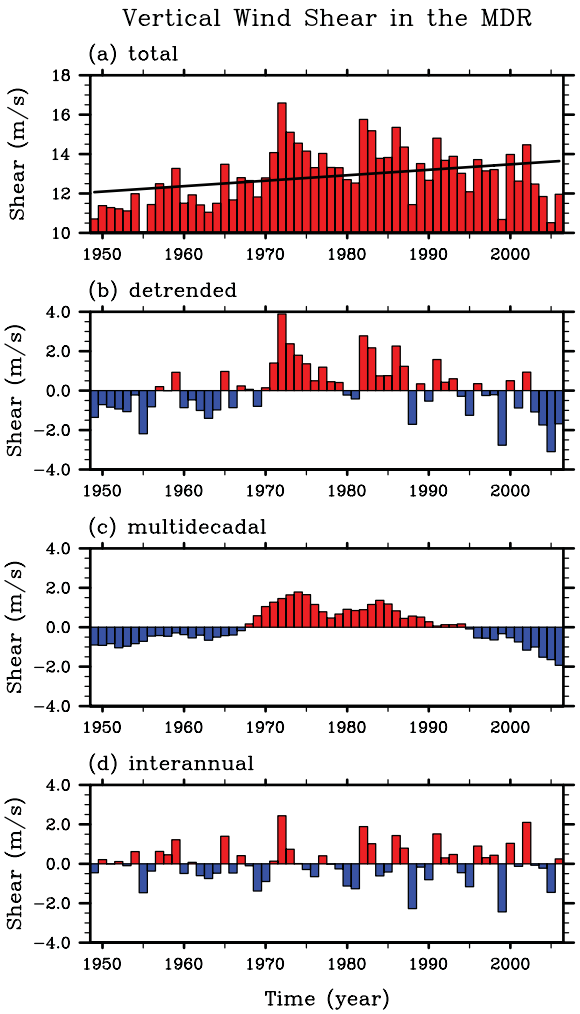


**Figure 8**. Time series of the vertical wind shear in the MDR (85°W-15°W, 10°N-20°N) for Atlantic hurricanes during JJASON. The vertical wind shear is calculated as the magnitude of the vector difference between winds at 200 mb and 850 mb. Shown are the (a) total, (b) detrended (removing the linear trend), (c) multidecadal, and (d) interannual variations. The multidecadal variability is obtained by performing a seven-year running mean to the detrened wind shear. The interannual variability is calculated by subtracting the multidecadal variability from the detrended wind shear. The black straight line in (a) is the linear trend that is fitted to the total wind shear.

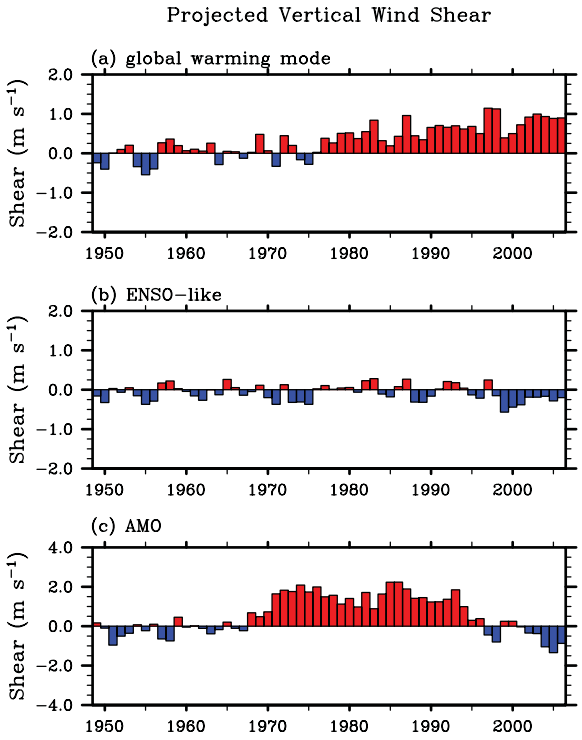


**Figure 9.** The projections of the vertical wind shear of Fig. 8a onto (a) global warming mode, (b) ENSO-like variation and (c) the AMO.

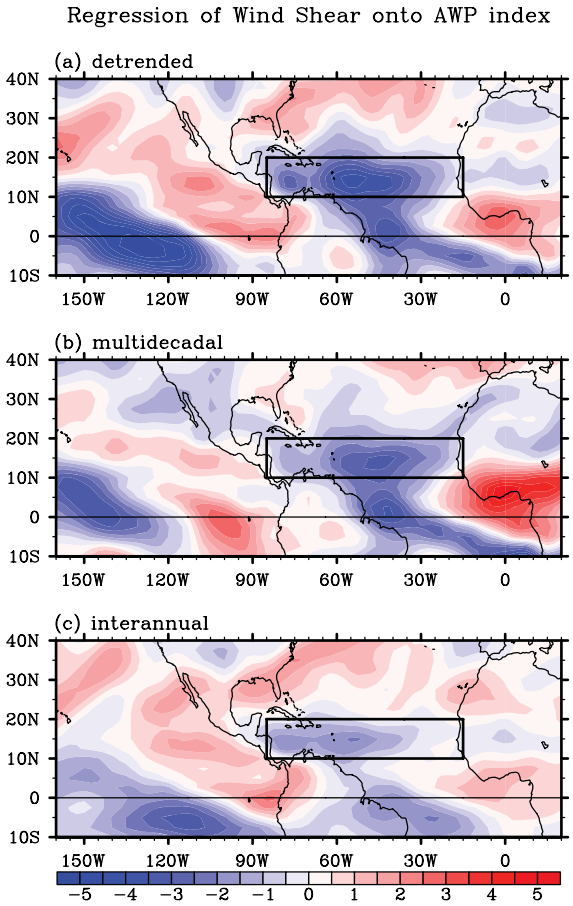


**Figure 10.** Regressions of the vertical wind shear during JJASON onto the AWP (a) detrended, (b) multidecadal, and (c) interannual indices. The AWP detrended, multidecadal, and interannual area indices in Figs. 2b-d are first normalized by their maxima. Then the regressions are calculated.

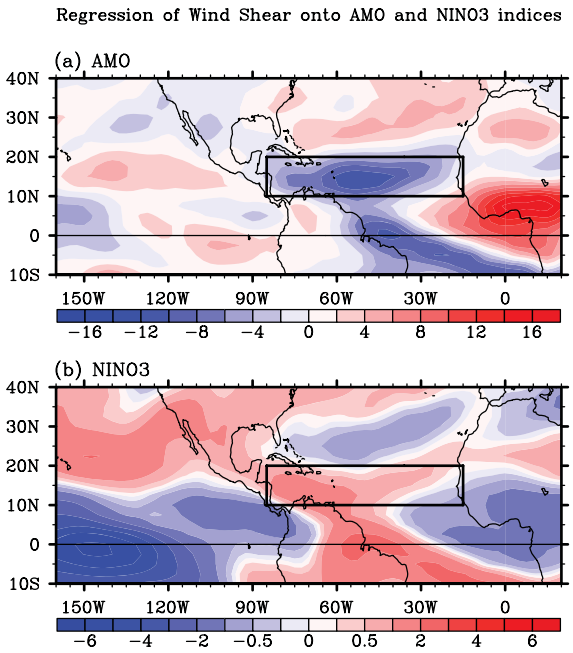


**Figure 11.** Regression coefficients of the vertical wind shear during JJASON onto (a) the AMO index and (b) the JJASON Nino3 SST anomalies.

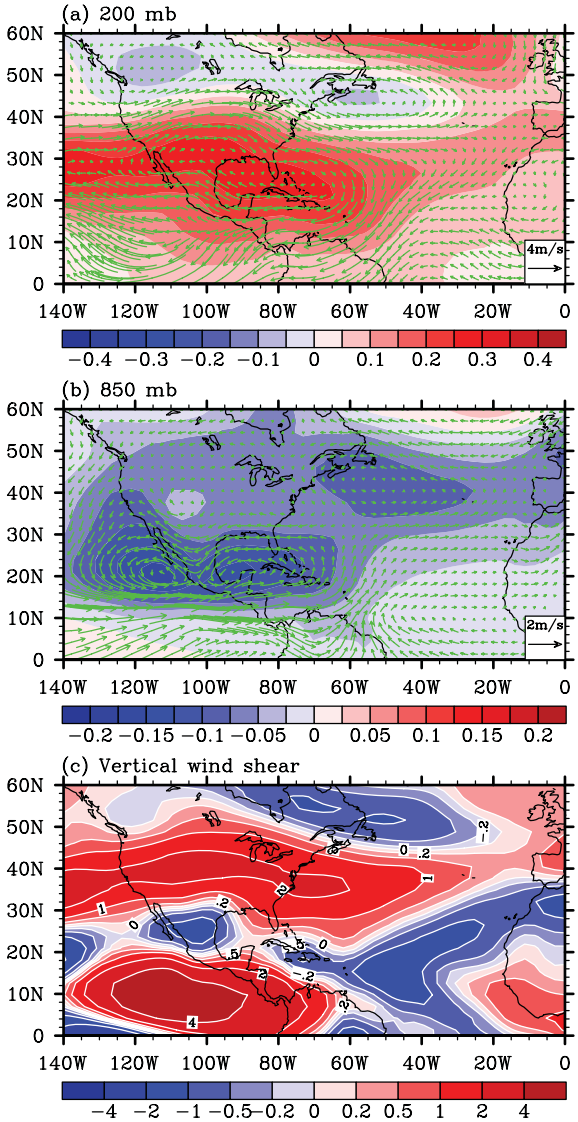


**Figure 12.** Atmospheric response to the LAWP and SAWP model ensemble runs (LAWP – SAWP) during June-November (JJASON). Shown are (a) geopotential height ($10^2$ m) and wind (m $s^{-1}$) at 200 mb, (b) geopotential height and wind at 850 mb, and (c) vertical wind shear (m $s^{-1}$) between 200 mb and 850 mb.

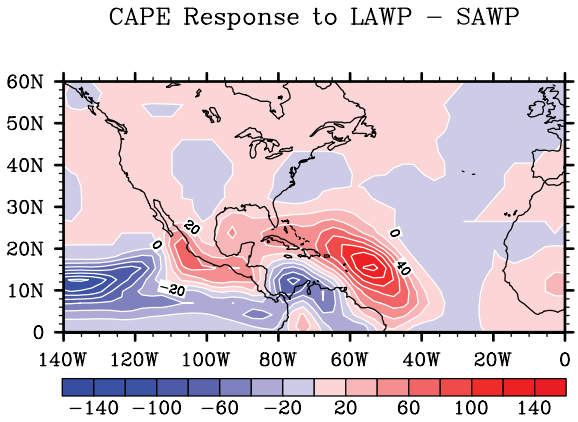


**Figure 13.** Response of Convective Available Potential Energy (CAPE; J/kg) to the LAWP and SAWP model ensemble runs (LAWP – SAWP) during June-November (JJASON).